EDITORIAL CSIC

Materiales de Construcción
76 (361), January-March 2026, e403
ISSN-L: 0465-2746, eISSN: 1988-3226
https://doi.org/10.3989/mc.2026.414525

ARTICLE

Strength, expansion and microstructural change of fly ash geopolymer mortars containing field Para rubber latex immersed in magnesium sulfate and sulfuric acid

Resistencia, expansión y cambio microestructural de morteros geopoliméricos de cenizas volantes con látex natural de caucho Para, sumergidos en sulfato de magnesio y ácido sulfúrico

A. Hawa
Infrastructure and Materials Innovation Research Unit, Department of Civil Engineering,
Princess of Naradhiwas University, (Narathiwat, Thailand)
Corresponding author: abideng.hawa@gmail.com; dr.abideng@pnu.ac.th, https://orcid.org/0000-0003-0800-9619

P. Salaemae
Infrastructure and Materials Innovation Research Unit, Department of Civil Engineering,
Princess of Naradhiwas University, (Narathiwat, Thailand)
preecha.s@pnu.ac.th, https://orcid.org/0009-0003-8695-8710

Abstract: Geopolymer mortar from fly ash (FA) and field Para rubber latex (FPRL) with alkaline activators was exposed to 5% magnesium sulfate and sulfuric acid for 90 days with compressive strength. Key parameters assessed include compressive strength, expansion, degradation products, and microstructural changes, analyzed using X-ray diffraction (XRD) and scanning electron microscopy (SEM). The study focused on heat-curing time and FPRL content. Samples were cured at 80°C for 0.5, 1, 2, or 4 hours, with FPRL added at 0%, 1%, 2.5%, and 5% by the weight of fly ash. The optimal mixture 1% FPRL with heat curing for 4 hours not only yielded the highest compressive strength but also effectively mitigated the loss of compressive strength caused by exposure to magnesium sulfate and sulfuric acid. Expansion decreased with higher FPRL content and longer curing times. SEM revealed diverse textures based on composition and a porous matrix caused by sulfuric acid erosion.

Keywords: Mortar; Alkaline activators; Fly ash; Microstructural.

Resumen: El mortero geopolimérico de cenizas volantes (FA) y látex de caucho natural Para (FPRL) con activadores alcalinos se expuso al 5% de sulfato de magnesio y a ácido sulfúrico durante 90 días para evaluar la resistencia a la compresión. Aparte de este parámetro, también se midieron expansión, productos de degradación y cambios microestructurales mediante difracción de rayos X (XRD) y microscopía electrónica de barrido (SEM). El estudio se centró en el tiempo de curado térmico y el contenido de FPRL. Las probetas se curaron a 80 °C por 0.5, 1, 2 o 4 horas, con FPRL al 0%, 1%, 2.5% y 5% respecto a la FA. La mezcla óptima (1% FPRL, 4 h de curado térmico) alcanzó la mayor resistencia y mitigó la pérdida causada por los agentes agresivos. La expansión disminuyó con más FPRL y mayor curado. Mediante SEM se observaron texturas diversas y una matriz porosa debida a la erosión del ácido sulfúrico.

Palabras clave: Mortero; Activadores alcalinos; Cenizas volantes; Microestructural.

Received: 04-04-2025 / **Accepted**: 08-11-2025 / **Published**: 25-06-2026

Citation: Hawa A, Salaemae P. 2026. Strength, expansion and microstructural change of fly ash geopolymer mortars containing field Para rubber latex immerse in magnesium sulfate and sulfuric acid. *Mater. Construcc.* 76(361):e403. https://doi.org/10.3989/mc.2026.414525

Supplementary information ↓

1. INTRODUCTION

Ordinary Portland cement (OPC) is used as the binder in the production of concrete for building materials. The demand for concrete is rising due to the development of infrastructure facilities, particularly in developing countries (1). However, it has been demonstrated that Portland cement concrete faces several issues, including durability problems when exposed to seawater (2-4) and substantial emissions of carbon dioxide throughout the production of cement (5). Previous studies have investigated the reduction of cement usage by employing waste materials as partial replacement for cement, including fly ash (6-8), rice husk ash (9-11), and palm oil ash (12-14), among others. However, these studies demonstrated only a partial replacement potential. Consequently, research has expanded to explore geopolymers, which enable the complete utilization of waste materials as base constituents, such as fly ash (15-17) or fly ash blended with waste materials (18-20).

Geopolymers exhibit excellent resistance to sulfate attack (21-23) and solid performance against acids (24-26). Curing temperature is pivotal in refining microstructure and enhancing mechanical behavior. In general, elevated-temperature curing accelerates geopolymerization relative to ambient curing (27, 28), and longer heat curing time similarly enhances the early-age compressive strength of geopolymer. Hawa *et al.* (29) reported that geopolymer mortars prepared from metakaolin (MK) achieved high early strength with longer heat curing time. Azarsa and Gupta (30) cured geopolymers using steam methods to achieve higher compressive strength compared to dry curing in an oven. The results show that the compressive strength achieved through steam methods was higher at every temperature (10-80 ºC). Therefore, high early strength can be guaranteed to some extent for the durability of geopolymer when it comes into contact with sulfate and acid solutions. Several researchers (31-33) reported that mortars and concrete with geopolymer binders had good resistance against acid and sulfate attacks, in addition to being environmentally friendly. This is because their low carbon emissions and ability to utilize industrial and agriculture waste as raw materials.

Fly ash is a raw material for geopolymer production due to its chemical composition rich in both SiO_2 and Al_2O_3 in significant quantities, enabling effective geopolymerization. Nevertheless, researchers have enhanced geopolymer properties derived from fly ash by incorporating other materials, such as palm oil ash (34, 35), metakaolin (36-38) and slag (39-41). Several researchers have incorporated natural rubber latex into geopolymer composites in order to improve specific material properties. This modification aims to optimize the performance of the geopolymer in various applications by enhancing targeted characteristics. Chindaprasirt and Ridtirud (42) reported that optimum of natural rubber latex for geopolymer mortars is 1.0 percent by weight of fly ash with improved strength properties and an increase setting time of geopolymer paste. Hawa *et al.* (43) observed that a geopolymer synthesized from fly ash and mixed with 1% natural rubber latex exhibited maximum compressive strength after being subjected to heat curing at 80°C for 4 hours. This process highlights the significance of both the latex concentration and the curing conditions in optimizing the mechanical properties of the material. Rath *et al.* (44) experimented with varying amounts of rubber latex, specifically 0.5%, 1%, 1.5%, and 2%, combined with calcined clay in a geopolymer. The findings indicated that increasing the proportion of natural rubber latex led to improved workability and reduced shrinkage. Rath (45) presented that natural rubber latex decreased water absorption and drying shrinkage with metakaolin based geopolymer concrete. Nonetheless, the current body of research on geopolymer materials incorporating natural rubber latex is still relatively sparse. This highlights the necessity for more comprehensive studies to be conducted in this area. Previous studies have primarily focused on investigating the strength, water absorption, setting time, and drying shrinkage. However, this study examined the durability of

geopolymer containing rubber latex when immersed in magnesium sulfate and sulfuric acid solutions, with emphasis on strength, expansion behavior, and microstructural characteristics. This scope represents a departure from previous research.

This study thus aimed to investigate the effects of field Para rubber latex in fly ash geopolymer matrix. The purpose of incorporating FPRL was to enhance the strength properties of geopolymer. The mechanical, durability properties, and microstructures of geopolymer towards magnesium sulfate and sulfuric acid attacks were studies. The finding in this study would offer an interesting way to used field Para rubber latex for the production of construction materials in the appropriate ratio and heat curing time. This study mixed field Para rubber latex with geopolymers to create a new construction-material innovation that is chemically resistant and environmentally friendly.

2. MATERIALS AND METHODS

2.1. Research methodology

Figure 1 presents a detailed and thorough flowchart that clarifies the methodology used in this study. This methodology involves several critical steps designed to systematically achieve the research objectives.

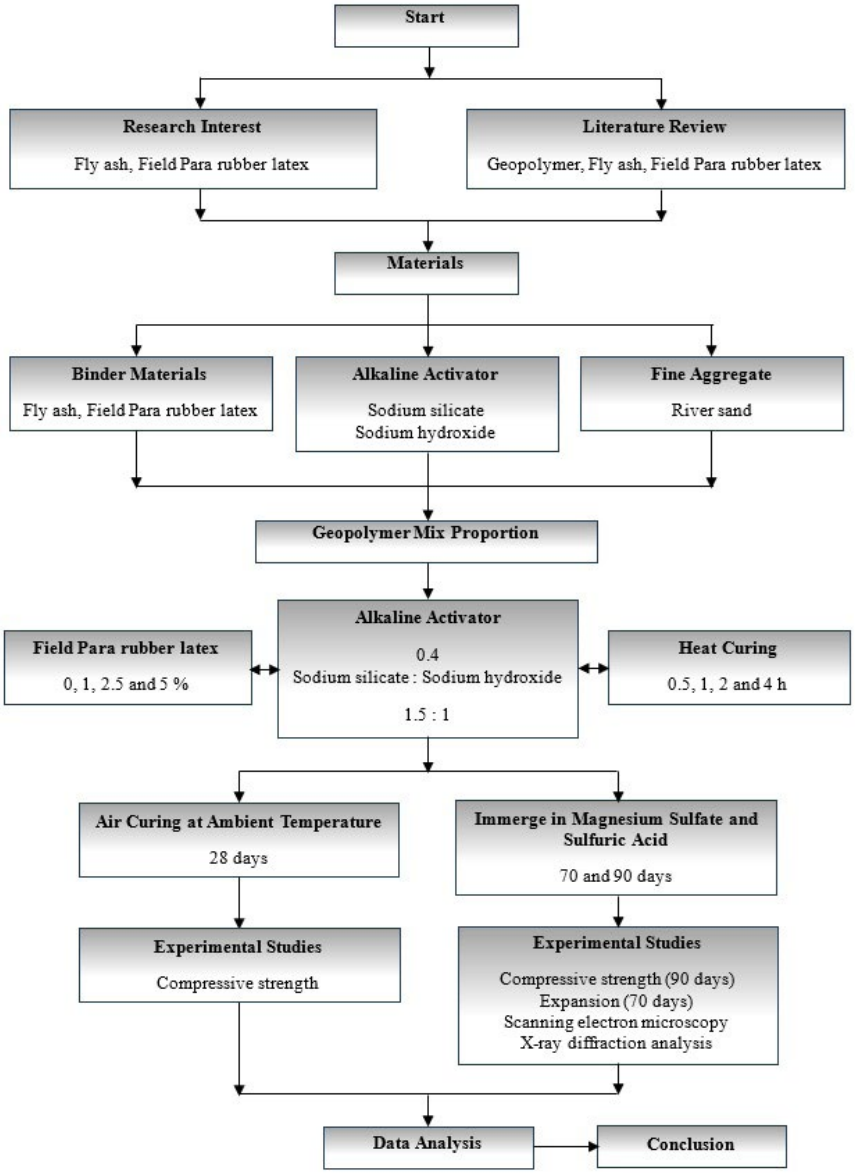

Figure 1. Flowchart of the research methodology.

2.2. Materials

Fly ash was obtained from the Mae Moh Electric Power Plant located in Lampang Province, northern Thailand. Table 1 and Figure 2 display the chemical and mineral compositions of the fly ash, respectively. The chemical composition of the fly ash was analyzed through X-ray fluorescence (XRF) analysis. which showed that the major oxides were silica (SiO_2) and alumina (Al_2O_3), while the CaO content was 12.5%. The particle size distribution of fly ash by Malvern laser particle size analyzer was shown in Figure 3. The average particle size of FA was 25.78 µm. The X-ray diffraction (XRD) patterns of fly ash are presented in Figure 2. The mineral phases in fly ash include quartz (SiO_2), anhydrite ($Ca(SO_4)$), and magnetite (Fe_2O_4). Sodium hydroxide (NaOH) and sodium silicate (Na_2SiO_3) were used as alkaline activators for geopolymerization reactions. Field Para rubber latex used in this study, derived from the RRIM 600 clone of rubber trees, was obtained from Narathiwat Province in Thailand. This FPRL is a suspension containing 35-40% total solid content. The particle size distribution of FPRL ranged from 0.04 to 4.0 µm (43). The chemical compositions of sodium silicate were 14.85 wt% NaO, 29.45 wt% SiO_2, and 55.70 wt% H_2O. Using sodium hydroxide of flakes is 99% purity. Geopolymer mortars were prepared using fine aggregates derived from natural river sand, which passed through ASTM sieve No. 4 according to ASTM C33/C33M (46). These aggregates had a particle size of less than 4.75 mm, a specific gravity of 2.55, and a fineness modulus of 2.58.

Table 1. The chemical composition of fly ash.

Oxide	SiO_2	Al_2O_3	CaO	Fe_2O_3	K_2O	SO_3	MgO	Na_2O	TiO_2
% by weight	45.3	23.0	12.5	9.4	2.3	2.7	1.7	1.0	0.4

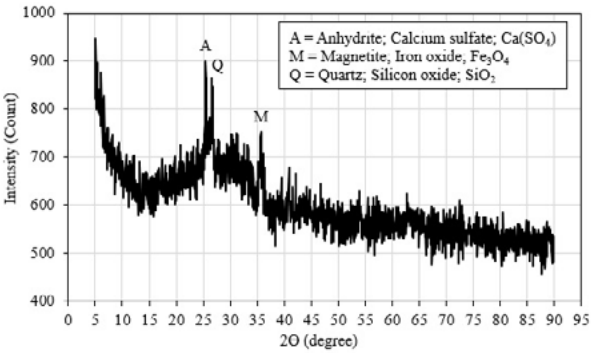

Figure 2. XRD pattern of FA.

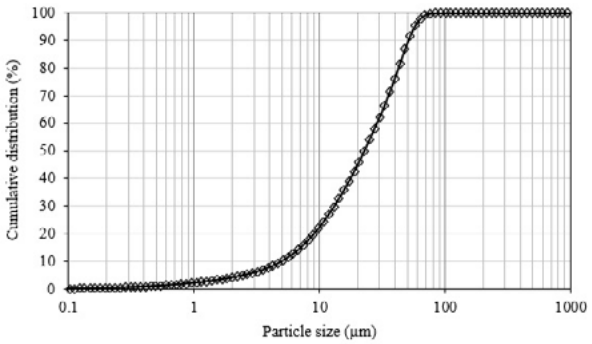

Figure 3. Particle size distribution of FA.

2.3. Sample preparation

In this research, the characteristics of geopolymer mortars were explored by analyzing the impact of varying FPRL and different heat-curing durations. Mixing ratio of geopolymer mortars based on FA. A total of sixteen mixtures were created by adjusting the FPRL content to 0%, 1%, 2.5%, and 5% by weight of fly ash. The geopolymer mortar compositions were specified with an alkaline-to-fly ash ratio of 0.4, a river sand-to-fly ash ratio of 2.75, and a sodium hydroxide-to- sodium silicate ratio of 1:1.5 by weight. These mixing proportions are detailed in Table 2. The preparation process for the geopolymer mortars consisted of four primary steps. Initially, FA and river sand were manually mixed for about 3 minutes to achieve an even distribution of materials. Next, sodium hydroxide, sodium silicate, and water were blended to create a uniform alkaline activator solution. This activator was then combined with the solid materials (FA and river sand) from the first step and mixed for around 3 minutes until a consistent slurry was formed. Finally, FPRL was incorporated into the mortar samples and mixed for 5 minutes. After mixing, the fresh geopolymer mortar was cast into 50×50×50 mm and 25×25×285 mm molds for compressive strength and expansion tests, respectively. The mortar was placed in acrylic molds, sealed with polyvinyl wrap, and heat-cured at 80 °C for 0.5, 1, 2, or 4 hours. Following thermal curing,

specimens were demolded and stored at room temperature until compressive strength testing. and immersed in magnesium sulfate and sulfuric acid until testing for compressive strength and expansion.

2.4. Characterization techniques

2.4.1. Compressive strength

The measured compressive strength of mortar specimen was assessed under three different conditions: 1. Curing at ambient temperature (air curing), 2. Immersion in a 5% magnesium sulfate ($MgSO_4$) solution, and 3. Immersion in a 5% sulfuric acid (H_2SO_4) solution. All specimens, measuring 50×50×50 mm, were initially subjected to heat curing at 80°C for durations of 0.5, 1, 2, and 4 h. Following the heat curing process, geopolymer mortars were maintained at room temperature for 28 days before testing with first condition. Compressive strength testing was performed in accordance with ASTM C109/C109M (47). For evaluating chemical resistance, after demolding, the specimens were immersed in 5% MgSO4 and 5% H_2SO_4 solutions. After 90 days of immersion, the compressive strength was measured to determine the extent of degradation. To assess the influence of each component, three samples were prepared and tested for each test type.

2.4.2. Expansion

Magnesium sulfate expansion of the geopolymer mortars was prevent mined by ASTM C1012/C1012M (48) utilizing 5 % $MgSO_4$. The expansion was determined with a length comparator in accordance with ASTM C490/C490M (49). For each mixture, three casting samples were tested. Throughout the course of this investigation, sulfate expansion tests were carried out on prismatic specimens measuring (25×25×285) mm. These specimens were kept at an ambient temperature of 30±2 °C and a relative humidity of 70±5%. Sulfate expansion tests were led during a time of 1 to 70 days (10 weeks). The typical level of development was determined in the accompanying Equation [1]:

$$L = \frac{L_x - L_i}{L_g} \times 100 \qquad [1]$$

Where
L = Length change (%).
Lx = Length at the testing age (cm).
Li = Length at the initial (cm).
Lg = Gauge length (cm).

2.4.3. Scanning electron microscopy (SEM) and X-ray diffraction (XRD) analysis

The synthesized geopolymer paste after immersed in magnesium sulfate and sulfuric acid for 90 days was investigated structural analysis with XRD and SEM. The XRD scans are performed at 2Θ = 5-90º with resolution using the clay and rock 0.4 program. For SEM analysis, small scraps of geopolymer paste were analyzed physical characteristic of surface. The sectioned specimens were air-dried and then sputter-coated with gold to enable microstructural imaging. Microstructure of the mortar matrix was investigated using a JEOL JMS-5800 LV scanning electron microscope (Japan).

3. RESULTS AND DISCUSSION

3.1. Compressive strength of geopolymer mortars

Figure 4 shows the compressive strength of mortar samples curing at ambient temperature at 28 days, samples immersed in magnesium sulfate and sulfuric acid. The specimens were exposed to 5% $MgSO_4$ and H_2SO_4 solution up to the age of 90 days. The effect of increasing FPRL in the geopolymer matrix on 28-day strength varies slightly when FPRL is added up to a maximum of 2.5% by weight. However, it was observed that 1% FPRL had highest compressive strength with ambient temperature curing at

28 days, especially, specimens were cured for 4 h. It is clearly that a 1% of FPRL represents the most suitable ratio for achieving optimal results. Adding 1% FPRL produced higher compressive strength at all heat curing durations, but when 2.5% latex or more was added, the compressive strength of geopolymer mortar decreased noticeably. The findings from this test closely resemble those obtained by Chindaprasirt and Ridtirud (42). According to Chindaprasirt and Ridtirud (42), the optimum natural rubber latex content was 1% by weight of high calcium fly ash to obtain geopolymer mortar with improved the compressive strength. A small particle size of latex could fill the pores of geopolymer matrix and make the specimen dens-compact. The filling of pores reduced the void in geopolymer matrix. Increasing the FPRL to 2.5% or higher leads to a reduction in compressive strength. This effect is attributed to the excessive FPRL content and the high surface tension associated with the latex. Moreover, the compressive strength of geopolymer from FA containing FPRL decreased with increasing FPRL content as dilution by water in the FPLR; as FPRL contains a large amount of water as a component, using a high quantity of FPRL results in increased water content in the geopolymer matrix. In similar research, Hawa *et al.* (50) investigated geopolymer mortars prepared from palm oil ash containing 1%, 3%, 5%, and 10% FPRL, cured at ambient temperature, and found that the 1% FPRL mix achieved the greatest 28 day compressive strength.

Table 2. Mix proportion of geopolymer mortars (FA 100%).

Mixture	FA (g)	FPRL (g)	Activator (g)		Water (g)	River sand (g)	Heat curing (h)
			SS = 1.5	SH = 1			
CT-0.5	100	0	24	16	25	275	0.5 (30 min)
CT-1	100	0	24	16	25	275	1
CT-2	100	0	24	16	25	275	2
CT-4	100	0	24	16	25	275	4
1L-0.5	100	1	24	16	25	275	0.5 (30 min)
1L-1	100	1	24	16	25	275	1
1L-2	100	1	24	16	25	275	2
1L-4	100	1	24	16	25	275	4
2.5L-0.5	100	2.5	24	16	25	275	0.5 (30 min)
2.5L-1	100	2.5	24	16	25	275	1
2.5L-2	100	2.5	24	16	25	275	2
2.5L-4	100	2.5	24	16	25	275	4
5L-0.5	100	5	24	16	25	275	0.5 (30 min)
5L-1	100	5	24	16	25	275	1
5L-2	100	5	24	16	25	275	2
5L-4	100	5	24	16	25	275	4

The compressive strength of geopolymer samples after immersion in the 5% $MgSO_4$ and 5% H_2SO_4 compared with geopolymer curing at ambient temperature as shown in Figure 4. Specimens subjected to immersion in a magnesium sulfate solution demonstrate superior compressive strength relative to those exposed to sulfuric acid, regardless of the mixture ratio or duration of heat curing. This indicates that magnesium sulfate may have a less aggressive impact on the compressive properties of the samples than sulfuric acid. This observation is supported by SEM images (see Figure 7-12), which reveal that samples soaked in a magnesium sulfate solution display a noticeably denser microstructure than those exposed to sulfuric acid. Obeng *et al.* (51) reported that the aluminosilicate gel formed during geopolymerization exhibits reduced susceptibility to magnesium sulfate attack. The increased density suggests a different interaction between the material and the magnesium sulfate solution, resulting in enhanced compressive properties. Additionally, the samples demonstrate greater compressive strength than geopolymer mortar blended with 2.5% and 5% FPRL that was cured in air for 28 days.

This suggests that magnesium sulfate immersion may significantly enhance the material's mechanical properties in comparison to latex-modified geopolymer mortars cured under standard conditions. This research examined the compressive strength of geopolymer mortars when subjected to $MgSO_4$ and H_2SO_4 exposure. The findings revealed that geopolymer mortars submerged in H_2SO_4 showed a decrease in compressive strength, with reductions ranging from 28.00% to 73.14%. It is believed that H_2SO_4 degrades the microstructure of cement concrete and geopolymers due to expansion caused by sulfate-containing compounds (52, 53). The greater deterioration observed with H_2SO_4 may be attributed to the migration of SO_4^{-2} ions within the geopolymer samples (54). Research by Aiken *et al.* (55) demonstrated that exposure to H_2SO_4 caused geopolymers to lose their inherent texture through leaching and gypsum deposition. Calcium sulfate hydrate, or gypsum, formation is a detrimental process within sulfuric acid-attacked geopolymers, leading to reduced compressive strength. Sulfuric acid reacts with calcium compounds in the geopolymer to form gypsum, a product that has a larger volume than the original material, causing internal stresses, microcracking, and ultimately, a significant loss of the geopolymer's load-bearing capacity (56, 57). The formation of gypsum is clearly evidenced by the SEM and XRD analysis results presented in Figures 10-12 and 14, respectively. Consequently, the deterioration caused by H_2SO_4 was more significant than that caused by $MgSO_4$. Moreover, Alzeebaree *et al.* (58) noted that the drop in compressive strength of geopolymer specimens under H_2SO_4 exposure stems from the breakdown of the aluminosilicate bridge (-Al-Si-O) within the geopolymer gel. Moreover, this -Al-Si-O linkage is a principal component of the matrix, underpinning gel strengthening and enhancing bonding among matrix constituents (59).

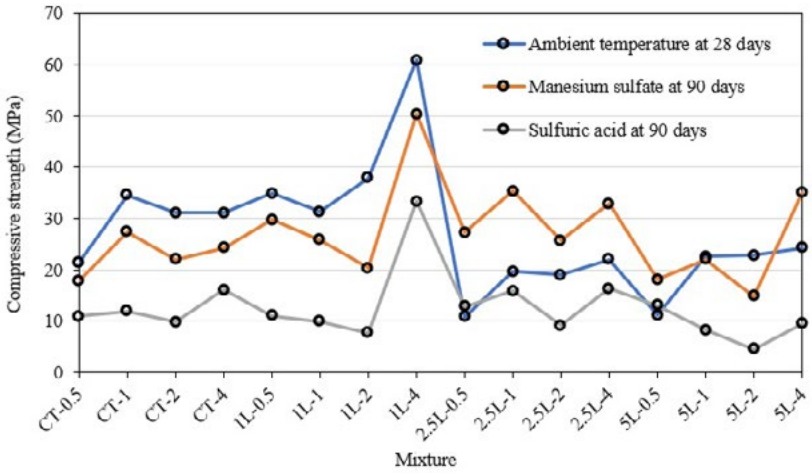

Figure 4. Compressive strength of geopolymer mortar.

3.2. Effect of FPRL and heat curing on compressive strength of geopolymer mortars immerse in magnesium sulfate and sulfuric acid

The results of compressive strength of geopolymer mortars immersion in $MgSO_4$ and H_2SO_4 are presented in Figures 4. The compressive strength exhibits a slight declining trend with an increase of FPRL. For example, the compressive strength of geopolymer containing 0%, 1%, 2.5% and 5% FPRL heat curing at temperature of 80 °C for 2h were 21.92, 20.30, 25.70 and 14.84 MPa, respectively. While specimen immersion in H_2SO_4 with 0%, 1%, 2.5% and 5% FPRL were 9.80, 7.68, 9.12 and 4.54 MPa, respectively. It was observed that geopolymer mortars an immerse in H_2SO_4 had lower than compressive strength comparison to in $MgSO_4$. This is because exposure to H_2SO_4 lost the intrinsic texture due to leaching and deposition of gypsum (55). In effect of heat curing, an analysis of the effects of heat curing clearly indicates that curing at 80 °C for 4 h. is the most effective method for mitigating compressive strength loss. This is attributable to curing at 80 °C for 4 hours, which enhances early-age compressive strength (29, 43), and especially, geopolymer mortar containing 1% FPRL. Hawa *et al.* (43) reported that extended heat curing markedly accelerated early-age strength development, as the geopolymer exhibited a densely compact matrix with fewer unreacted raw materials.

3.3. Sulfate expansion

The durability of the expansion of geopolymer mortars was analyzed after immersion in magnesium sulfate solution (5% $MgSO_4$) for 70 days. In Figures 5 and 6, the testing of expansion was considered in two affect such as effect of heat curing time and FPRL content, respectively. Figures 5(a) and 5(b) illustrate the expansion of geopolymer mortars control (CT) and containing 1% FPRL (1L), respectively. Geopolymer mortar bar of rapid expansion is observed after one day of immersion in $MgSO_4$ solution. Because the CT and 1L mixtures contain a low amount of water in the system (due to no water from FPRL (CT) and only a small amount of water from 1% FPRL (1L), the system retains little water after heat curing. When the samples were immersed in magnesium sulfate solution, rapid expansion occurred in the early stages. However, the expansion value was similarly significant with specimen heat curing for 0.5 and 1 h, while geopolymer samples heat curing for 2 and 4 h give clearly lower expansion with all mix proportions. This is because prolonged heat curing clearly accelerated high early strength. Sata *et al.* (60) observed that specimens with low compressive strength at an early age exhibit a pronounced tendency for significant high expansion during the same period. Similarly, when using 2.5% and 5% FPRL, as shown in Figures 5(c) and 5(d), respectively, it is evident that geopolymer mortar specimens exhibited lower expansion values after 2 and 4 h of heat curing compared to those cured for 0.5 and 1h. Notably, longer curing durations resulted in reduced expansion, likely due to improved reaction efficiency, which consequently yielded higher compressive strengths. Additionally, it is plausible that higher FPRL content contributed to reduced expansion, because FPRL has water as its main component, when mixed into the geopolymer, it leads to an increased water content within the geopolymer matrix and thus lower expansion.

In the Figure 6, the expansions are presented for mixes containing 0%, 1%, 2.5%, and 5% FPRL that were heat-cured at 80 °C for 0.5, 1, 2, and 4 hours, and extended curing durations reduced the expansion. For example, the CT and 1L samples (Figure 6(c)) cured for 2 h had similar expansion behavior with high expansion at early age test sample. It is noteworthy that after 14 days, the expansion values were nearly identical for the CT and 1L specimens. In contrast, geopolymer samples incorporating 2.5% FPRL (2.5L) exhibited expansion values similar to those with 5% FPRL (5L). This was because the incorporation of higher amounts of FPRL resulted in increased water content within geopolymer matrix, as FPRL contains a significant proportion of water in its mixture. This led to lower expansion values.

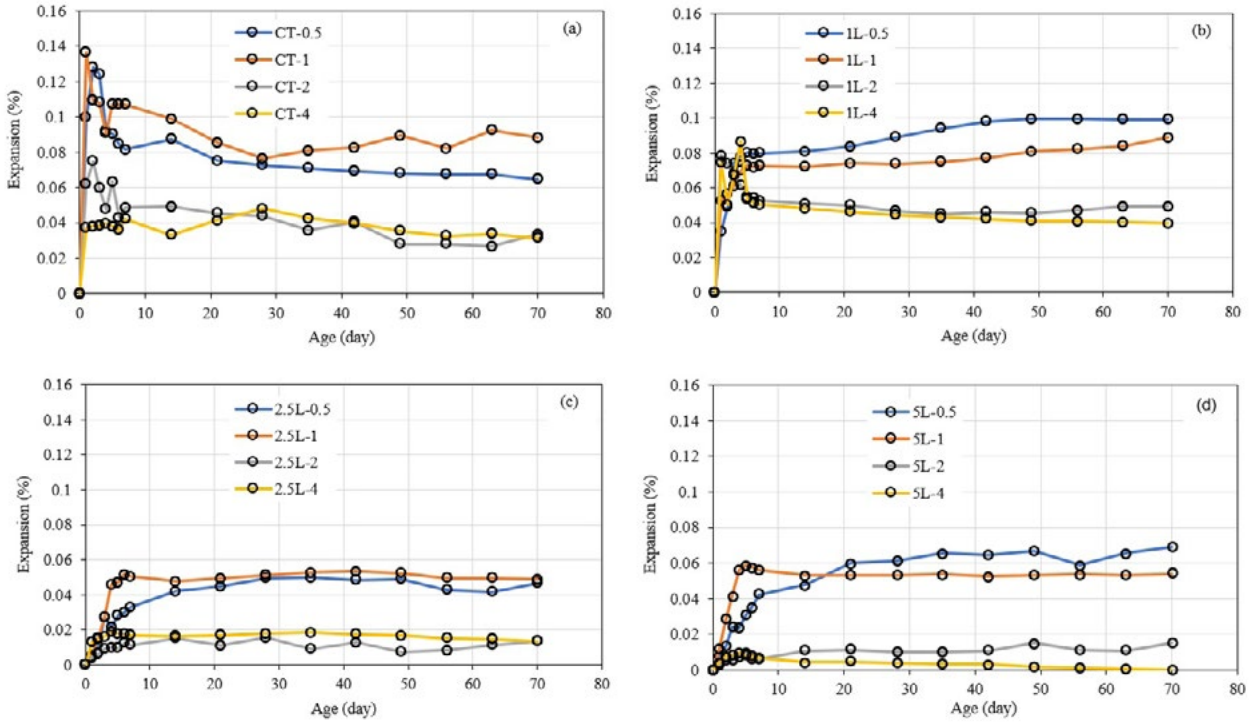

Figure 5. Expansion of geopolymer mortars immersion in magnesium sulfate, effect of heat curing; (a) without FPRL, (b) 1% FPRL, (c) 2.5% FPRL, and (d) 5% FPRL.

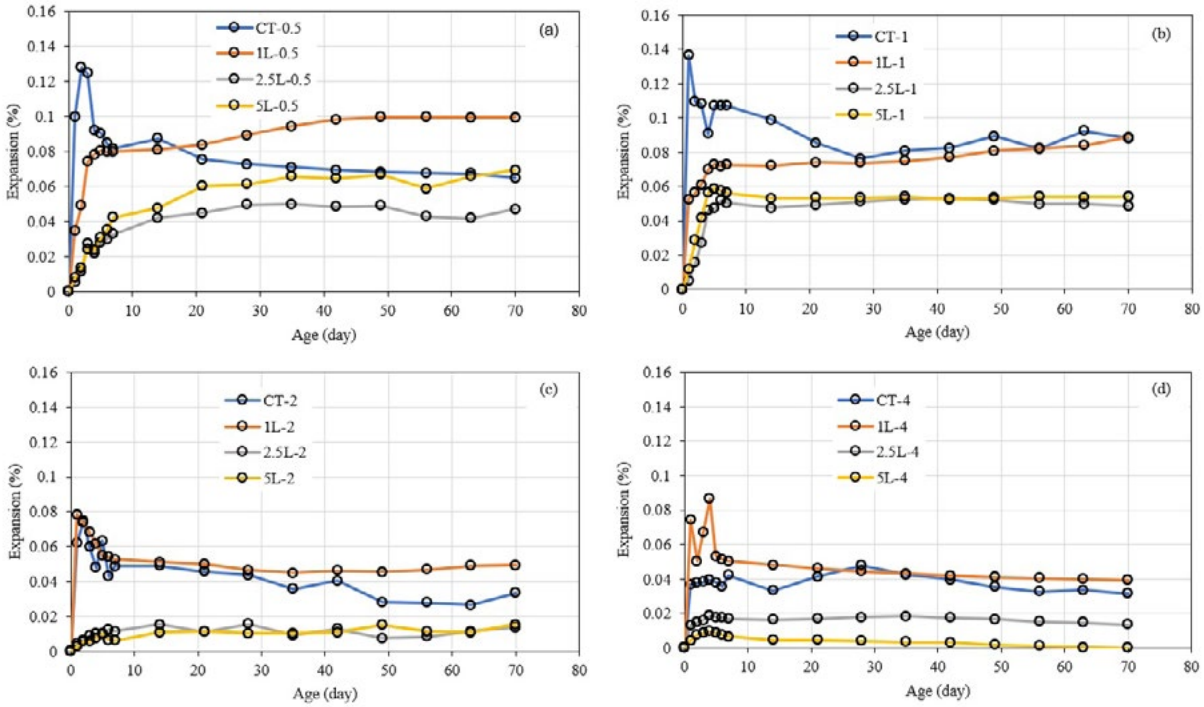

Figure 6. Expansion of geopolymer mortars immersion in magnesium sulfate, effect of FPRL; (a) 0.5 h, (b) 1 h, (c) 2 h, and (d) 4 h.

3.4. SEM

3.4.1. Magnesium sulfate

In this section, only the effect of binder and heat curing on scanning electron microscope (SEM) of mortars after 90 days of exposure of 5% $MgSO_4$ is studied. Geopolymer samples were cured at 80 °C for 0.5, 1 and 4 h. Figures 7-9 show SEM micrographs of specimen heat cured for 0.5, 1 and 4 h respectively with exposed to $MgSO_4$ attack. Figure 7 presents representative morphologies of the geopolymerization products. The specimens display fine pores throughout the microstructure. Pore globules within the matrix are roughly micrometer-scale in diameter, but these spherical features are not interconnected. The micrographs indicate an inherently porous texture, and the particulates visible in the SEM images correspond to silica (61-63). The 1L-0.5, 2.5L-0.5 and 5L-0.5 specimens clearly exhibited unreacted raw materials. No geopolymerization phases were observed on the silica globular surfaces, and the interfacial transition zone between these globules and the surrounding matrix showed voids around the silica particles. Furthermore, it was also found that geopolymer exhibited micro cracks at all mixing ratios. Geopolymer subjected to heat curing for 0.5 and 1 hour exhibited a similar texture, as shown in Figures 7 and 8, respectively. According to Bakharev (64) the exposure solution caused $MgSO_4$ to diffuse over the surface of geopolymer samples. Calcium was transferred from the specimen to the surface area at the same moment. The XRD patterns showed the formation of crystals of gypsum (Calcium Sulfate Hydrate) encrusted in the geopolymer phase ($CaSO_4 2H_2O$) (see Figure 13). It is noteworthy that all mixing ratios exhibited a significant number of pores and cracks, which contributed to a reduction in the compressive strength of geopolymer mortars. The $MgSO_4$ deterioration of fly ash based geopolymer performance primarily arises from a weak cementation mechanism and gypsum induced cracking. The weak cementation stems from Mg^{2+} replacing species in C-A-S-H and N-A-S-H, converting them to M-A-S-H with inferior mechanical properties and bonding capacity (65). However, as observed in Figure 9(a), the geopolymer matrix appeared dense and homogeneous, with no visible cracks, which is consistent with the compressive strength test results showing that Sample 1L-4 exhibited the highest compressive strength.

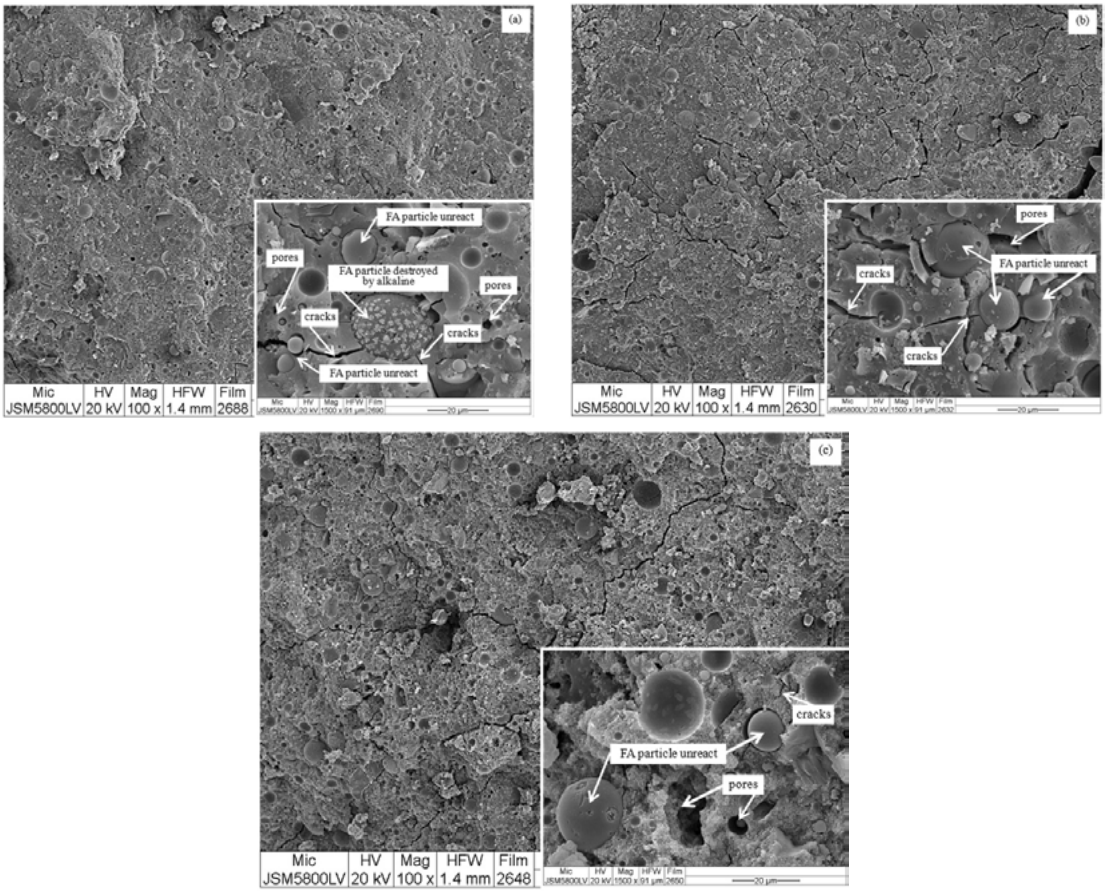

Figure 7. SEM images of geopolymer mortar with immersion in magnesium sulfate, heat curing for 0.5h; (a) 1L-0.5, (b) 2.5L-0.5 and (c) 5L-0.5.

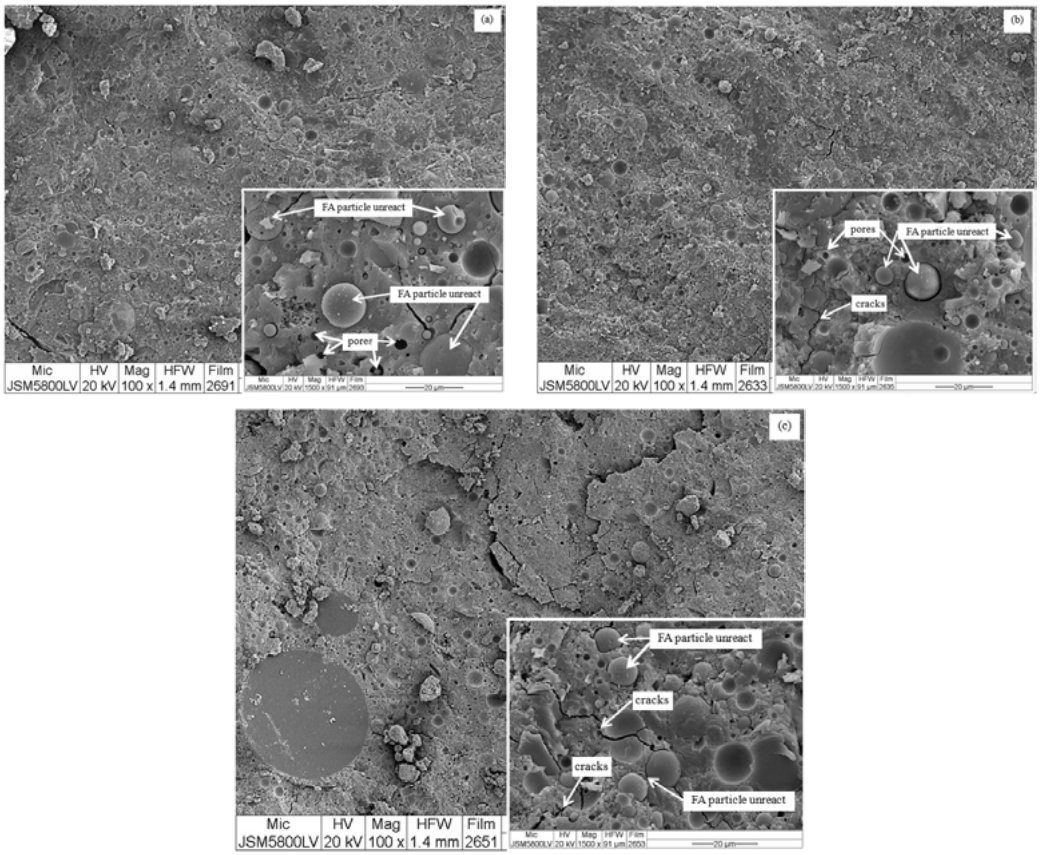

Figure 8. SEM images of geopolymer mortar with immersion in magnesium sulfate, heat curing for 1h;

(a) 1L-1, (b) 2.5L-1 and (c) 5L-1.

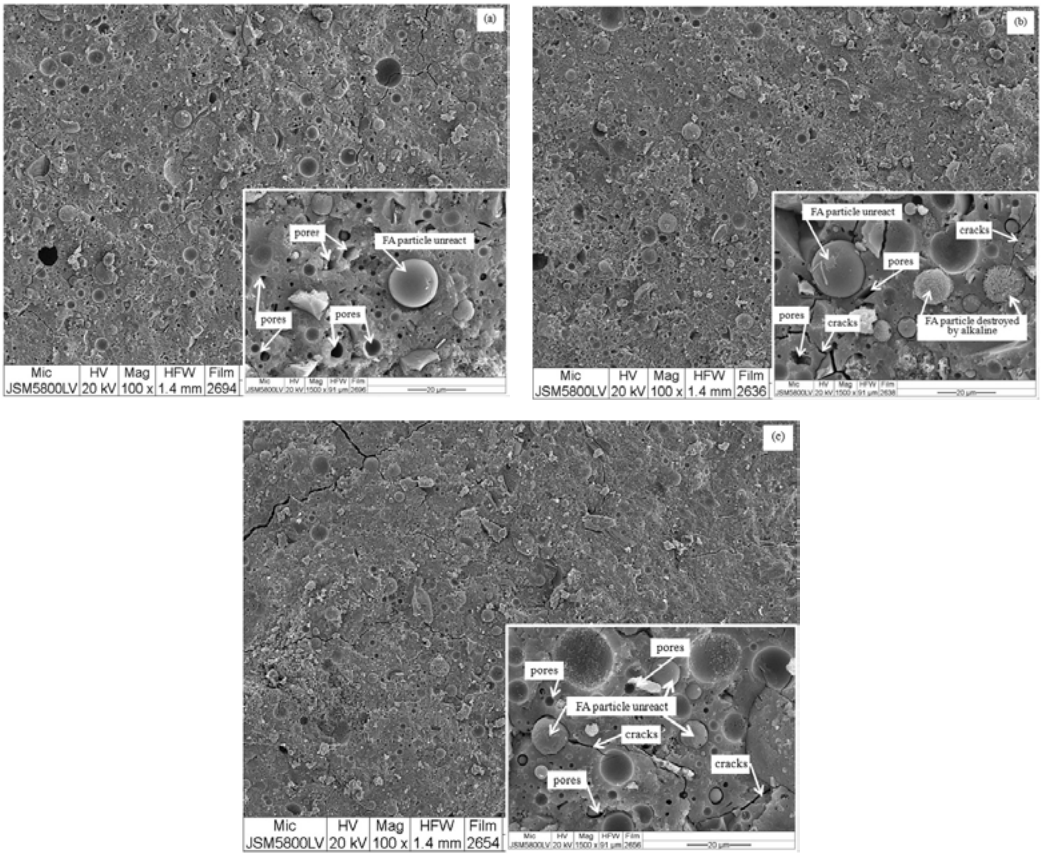

Figure 9. SEM images of geopolymer mortar with immersion in magnesium sulfate, heat curing for 4h; (a) 1L-4, (b) 2.5L-4 and (c) 5L-4.

3.4.2. Sulfuric acid

Figures 10-12 presents the SEM images of different geopolymer specimen immersed in sulfuric acid solution for 90 days. The specimens exposed to 5% H_2SO_4 solution for 90 days were observed as micrographs and compared with different condition. As seem from Figures 10-12, partials unreacted fly ash particles as well as loose and non-homogeneous were observed in geopolymer matrix. The microstructural analysis conducted using a scanning electron microscope revealed the presence of a significant amount of gypsum crystals dispersed throughout all mixing ratios and curing durations. The extensive formation of gypsum directly resulted in a substantial reduction in the compressive strength of the geopolymer samples. The gypsum crystals formed were isolated, rod-shaped, and lacked interconnection. The excessive presence of gypsum led to a heterogeneous geopolymer matrix. It is noteworthy that the incorporation of 5% FPRL results in a significantly higher dispersion of gypsum crystals throughout geopolymer matrix, which is more pronounced compared to the samples containing 1% and 2.5% FPRL. The abundant presence of gypsum crystals corresponds to the results of the XRD analysis (see Figure 14). When observing the larger image (x100), it was evident that the geopolymer mortar in all mixing ratios exhibited a porous, degraded texture, which was one of the factors contributing to the reduction in compressive strength after immersion in sulfuric acid. However, sample 1L-4 displayed a denser internal texture compared to other mixtures. Despite containing a significant amount of flake-like debris, it did not exhibit the network-like porosity observed in other samples, resulting in a higher compressive strength. Yang *et al.* (66) reported that among the geopolymer morphologies affected by H_2SO_4, gypsum was the most significant corrosion product. Xie *et al.* (67) demonstrate that gypsum crystals clog the pores of the geopolymer matrix and compact the microstructure of the specimen, preventing further H_2SO_4 corrosion (68). Considering the components of natural rubber latex, which include rubber particles, proteins, resins, carbohydrates,

and inorganic substances primarily composed of oxygen (O), nitrogen (N), carbon (C), and hydrogen (H), it is unlikely to have any effect on gypsum formation, which requires calcium ions and sulfate ions as its primary components. It is possible that increasing the amount of natural rubber latex increases the water-to-fly ash ratio due to the high water content in fresh latex. The increase in the water-to-fly ash ratio results in more pores forming in the hardened geopolymer, which enhances its permeability. This allows sulfuric acid to penetrate deeper into the geopolymer mortar, leading to more intense chemical reactions and greater formation of gypsum crystals. However, this study revealed that a significant amount of gypsum formed after immersion in sulfuric acid, as clearly observed in the SEM images and confirmed by XRD analysis, as shown in Figure 14. This formation negatively impacted the compressive strength of geopolymer mortars.

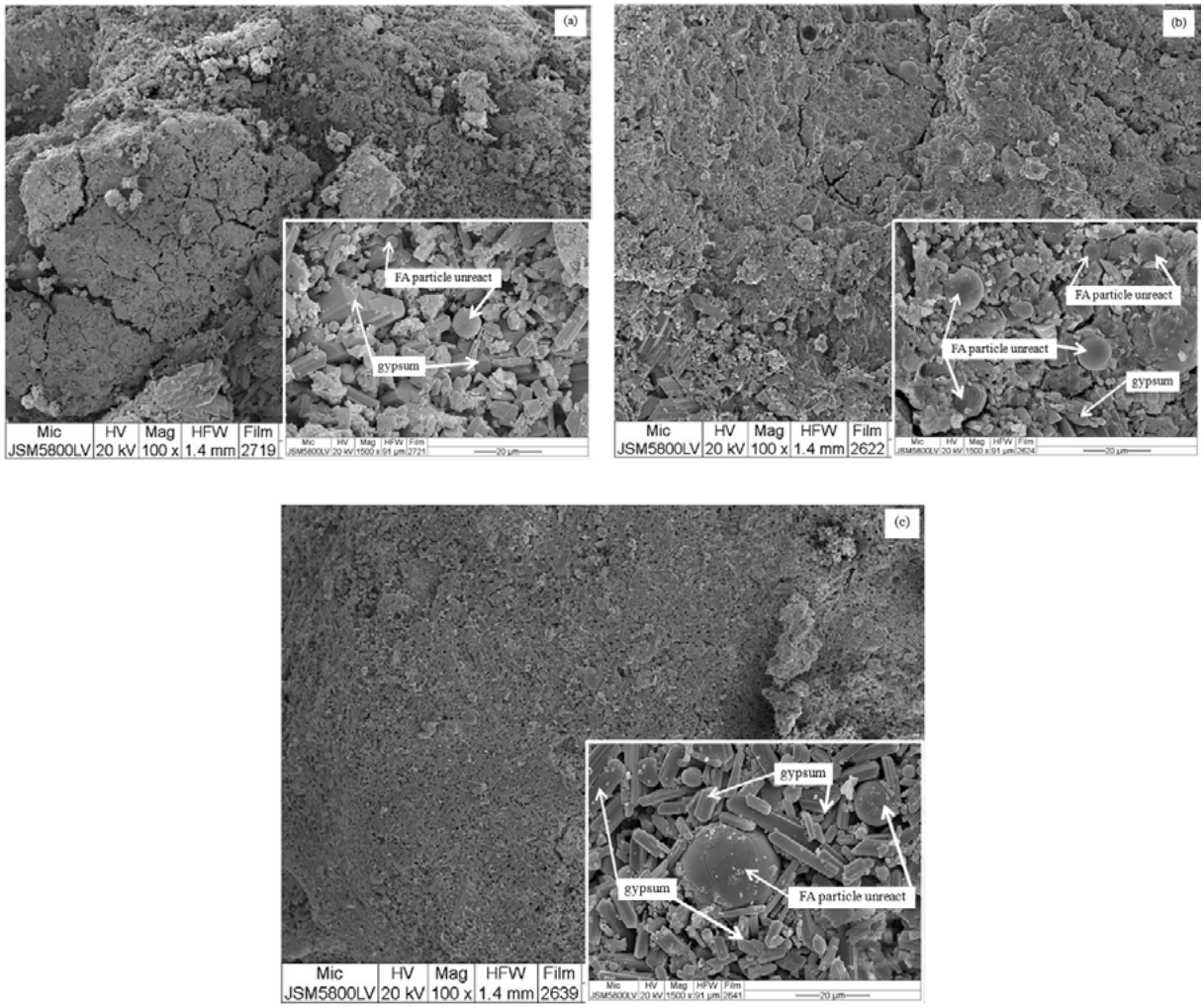

Figure 10. SEM images of geopolymer mortar with immersion in sulfuric acid, heat curing for 0.5h; (a) 1L-0.5, (b) 2.5L-0.5 and (c) 5L-0.5.

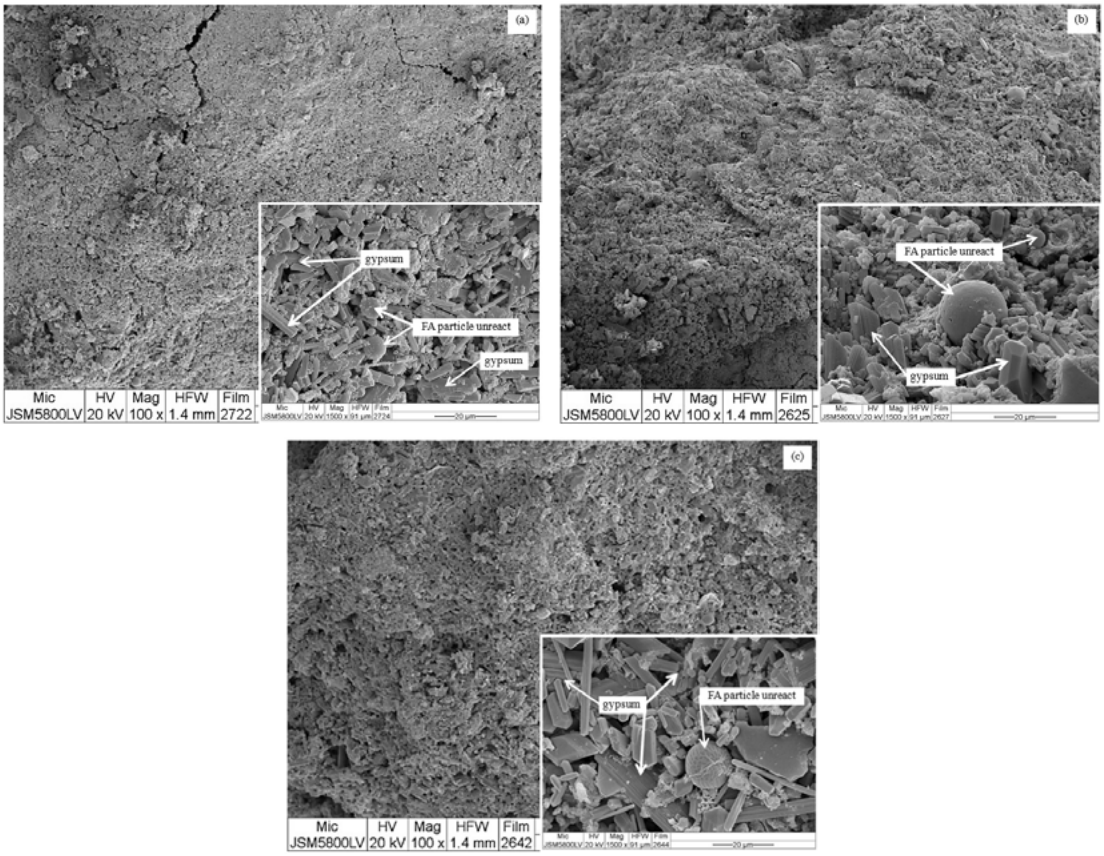

Figure 11. SEM images of geopolymer mortar with immersion in sulfuric acid, heat curing for 1h; (a) 1L-1, (b) 2.5L-1 and (c) 5L-1.

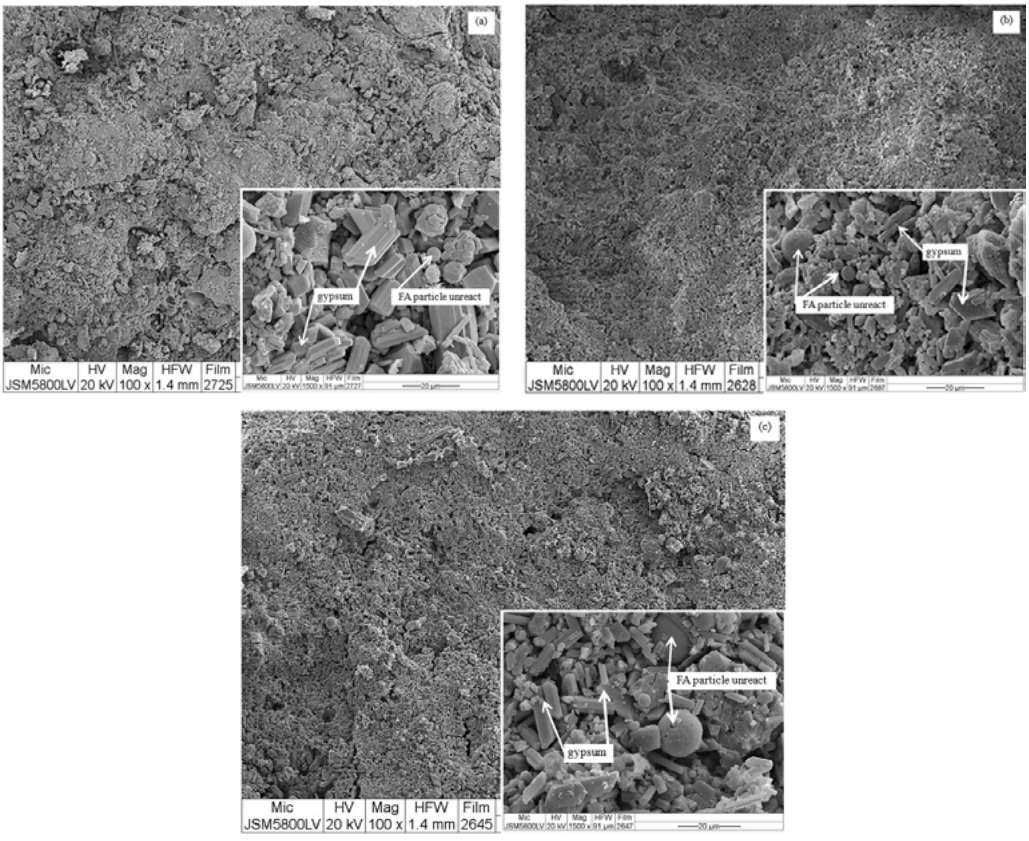

Figure 12. SEM images of geopolymer mortar with immersion in sulfuric acid, heat curing for 4h; (a) 1L-4, (b) 2.5L-4 and (c) 5L-4.

3.5. XRD PATTERN

3.5.1. Immersion in magnesium sulfate

The mineral compositions of the degradation of different samples with vary of FPRL and heat curing time after 90 days of exposure to magnesium sulfate solutions were analyzed and the resulted are shown in Figure 13. For geopolymer paste samples, the main peaks mainly related to Gypsum (Calcium Sulfate Hydrate; $CaSO_4 2H_2O$), Quartz (Silicon Oxide; SiO_2), and Magnetite (Iron Oxide; Fe_3O_4), indicating that the N(C)-A-S-H gel product was decomposed in the magnesium sulfate environment, the main alkaline activation products of FA are amorphous N(C)-A-S-H gels (69). In addition, the intensity of the gypsum and quartz peaks in geopolymer pastes exposed to magnesium sulfate revealed that samples with a higher FPRL content exhibited more pronounced peaks compared to those with a lower FPRL content. Furthermore, geopolymer pastes subjected to shorter heat curing durations demonstrated more distinct gypsum and quartz peaks than those subjected to longer heat curing periods. This is because prolonged heat curing promotes a more complete geopolymerization reaction (70), enabling the geopolymer to achieve higher compressive strength in a shorter time frame (after demolding). As a result, when immersed in magnesium sulfate, these samples produced less gypsum. The absence of anhydrite (calcium sulfate; $CaSO_4$) in the geopolymer samples, despite its clear detection in the fly ash, indicates that the N(C)-A-S-H phase in the paste was decalcified or decomposed, providing the calcium required for gypsum production. Furthermore, Mg^{2+} ions can cause calcite to partially dissolve (71), which explains why this phase is less intense.

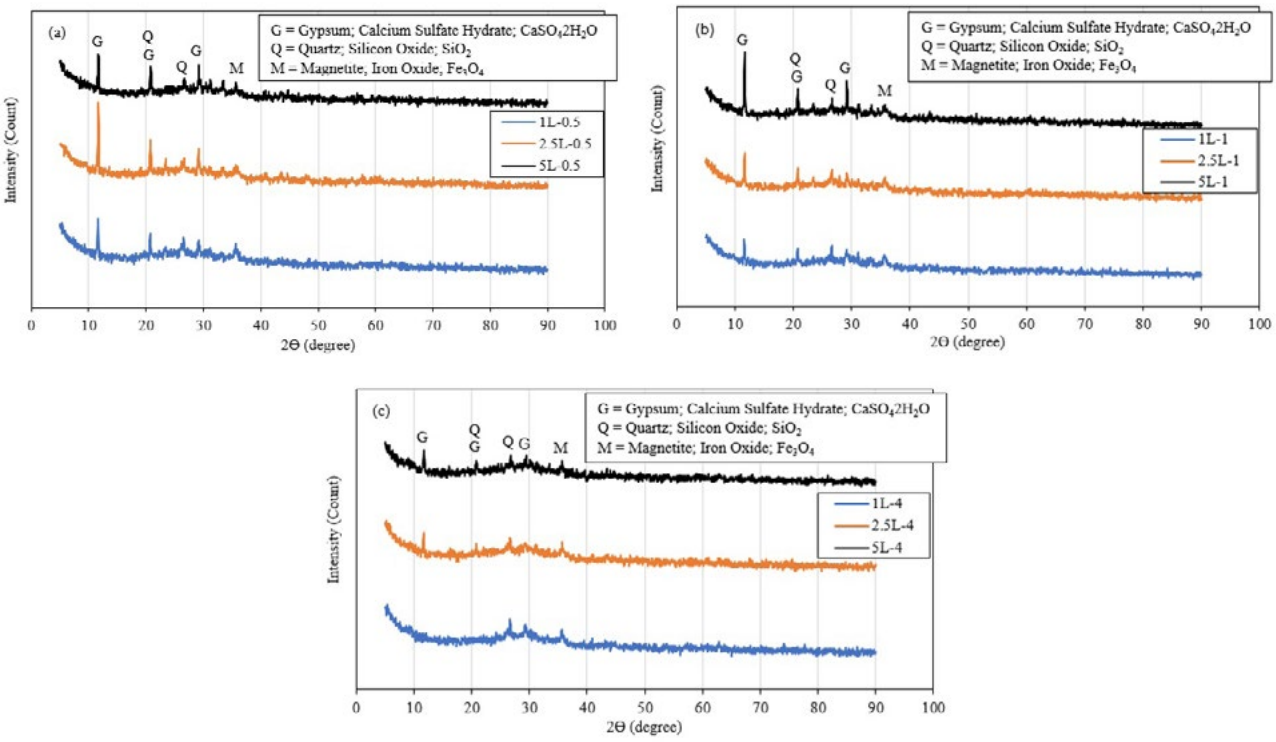

Figure 13. XRD pattern of geopolymer paste immersion in magnesium sulfate; (a) heat curing for 0.5 h (b) heat curing for 1 h and (c) heat curing for 4h.

3.5.2. Immersion in sulfuric acid

Figure 14 presents the XRD patterns of geopolymer paste after they were exposed to 5% H_2SO_4 for 90 days. The samples display the main crystal of gypsum. When comparing geopolymer pastes immersed in sulfuric acid and magnesium sulfate, it was found that immersion in sulfuric acid resulted in a more pronounced formation of gypsum compared to immersion in magnesium sulfate, across all mix ratios and

heat curing time. This demonstrates that sulfuric acid reacts well with the products of geopolymerization, resulting in the formation of a large amount of gypsum. Gypsum exhibits a markedly stronger presence in these systems, irrespective of heat curing duration or FPRL dosage. The anhydrite and magnetite phases in the peat were no longer present, but a crystal phase of gypsum emerged. Chen et al., (72) explained that calcium carbonate reacts with sulfuric acid, resulting in the formation of gypsum. The wide hump observed in geopolymer mixes within the range of approximately 20 to 35° 2Θ suggests the existence of aluminosilicate gel and amorphous silicate phases (73). The diffraction peak corresponding to gypsum was detected at 2Θ = 11° and 29° (approximately), consistent with findings documented in prior studies (74). In this case, the N-A-S-H gel which is formed in fly ash system. It was also detected that at the position around 21° 2Θ, gypsum and quartz were prominently observed. According to Aiken et al., (55) there was a peak at around 21° 2Θ that showed the presence of both quartz and gypsum.

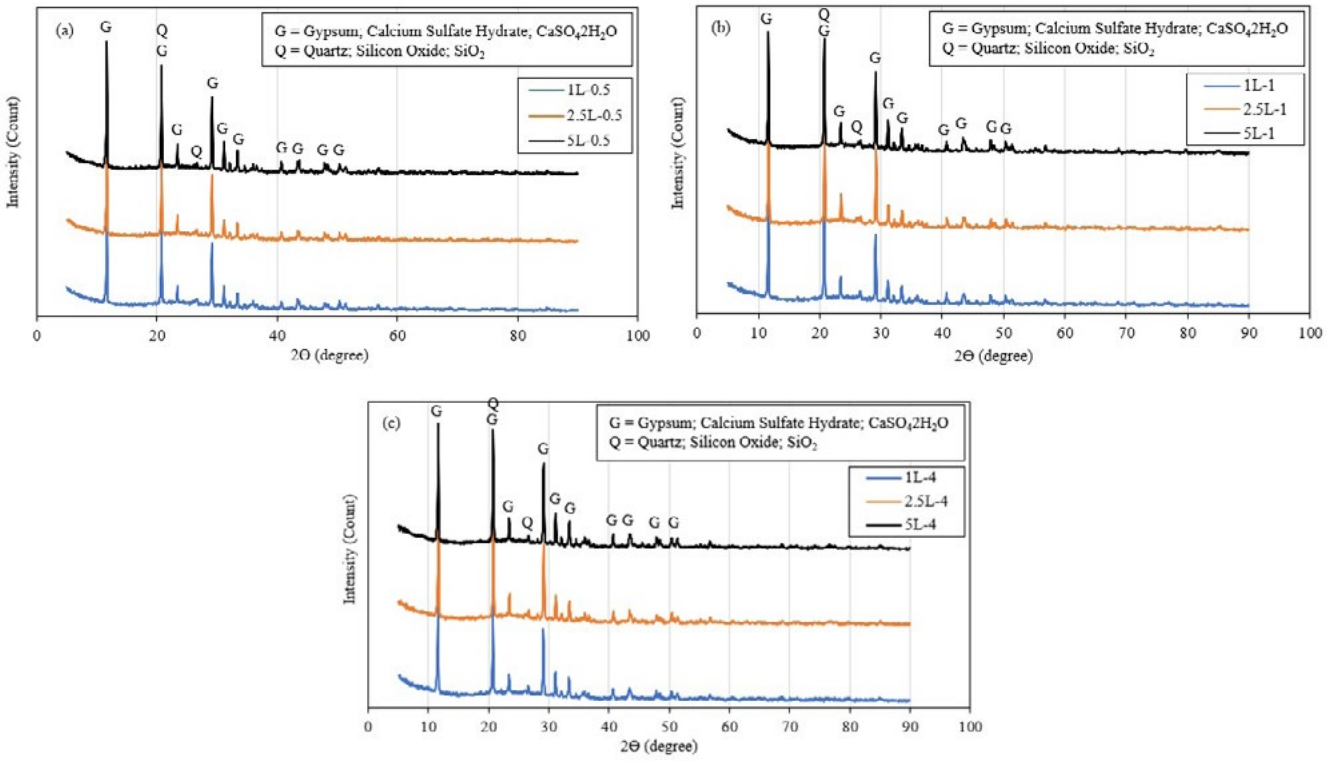

Figure 14. XRD pattern of geopolymer paste immersion in sulfuric acid;
(a) heat curing for 0.5 h (b) heat curing for 1 h and (c) heat curing for 4h.

4. CONCLUSIONS

This study examined accelerated deterioration in geopolymer mortars containing field Para rubber latex and varying heat-curing durations by exposing them to aggressive magnesium sulfate and sulfuric acid environments. Degradation was evaluated through residual compressive strength and expansion measurements, along with the study of microstructural changes and reaction products with magnesium sulfate and sulfuric acid. The brief conclusions are presented below.

1. Geopolymer mortars containing 1% FPRL achieved the highest compressive strengths across all tested curing periods, with the maximum strength observed after 4 hours of curing.

2. Geopolymer mortars containing 1% FPRL and heat cured for 4 hours provides the best protection against degradation from magnesium sulfate and sulfuric acid.

3. The compressive strength of geopolymer mortar specimens after being exposed to 5% $MgSO_4$ and H_2SO_4 separately. The deterioration of specimens exposed to H_2SO_4 was higher than the

specimens exposed to $MgSO_4$. The maximum compressive strengths of 50.44 and 33.43 MPa were observed for 1% FPRL incorporated fly ash geopolymer mortars exposed to $MgSO_4$ and H_2SO_4, respectively, heat curing for 4 hours.

4. Submerging geopolymer mortar in $MgSO_4$ and H_2SO_4 solutions, the specimens heat cured for 2 and 4 hours exhibited less expansion compared to those heat-cured for 0.5 and 1 hour. Specifically, the specimens mixed with 2.5% and 5% FPRL exhibited the lowest expansion values.

5. Microstructural analysis of acid-induced deterioration showed the formation of needle-like calcium sulfate (gypsum) crystals resulting from intense exposure to H_2SO_4. Consequently, the leaching of Ca or Na cations from the aluminosilicate gel leads to its degradation, which in turn compromises the microstructure of the fly ash geopolymer.

Supplementary information ↑

Funding sources

The authors express their heartfelt thanks for the financial assistance granted by National Research Council of Thailand.

Supplementary material

Not applicable.

Data availability

Not applicable.

Acknowledgements

The authors also extend their appreciation to the Infrastructure and Materials Innovation Research Unit and the Department of Civil Engineering, Faculty of Engineering, Princess of Naradhiwas University, Amphur Muang, Narathiwat, for kindly allowing the use of their facilities.

Authorship contribution statement

Abideng Hawa: Conceptualization, Data cleansing, Formal analysis, Funding raising, Research, Methodology, Project administration, Resources, Supervision, Validation, Visualization, Write-up-original draft, Write-up- review & editing.

Preecha Salaemae: Conceptualization, Funding raising, Methodology, Resources, Supervision.

Competing interests

The authors declare that they have no known financial conflicts of interest or personal relationships that could have influenced the work reported in this article.

Statement on the use of Artificial Intelligence

Not applicable.

REFERENCES

1. Fateh B. 2022. How does concrete and cement industry transformation contribute to mitigating climate change challenges?. Res. Conser. Rec. Adv. 15:200084. https://doi.org/10.1016/j.rcradv.2022.200084

2. Dimitrr VV, Mark GS. 2003. Life-cycle cost analysis of reinforced concrete structures in marine environments. Struc. Saf. 25(4):343-362. https://doi.org/10.1016/S0167-4730(03)00014-6

3. Li D, Li LY, Wang X. 2019. Chloride diffusion model for concrete in marine environment with considering binding effect. Mar. Struct., 66:44-51. https://doi.org/10.1016/j.marstruc.2019.03.004

4. Paiva H, Velosa A, Cachim P, Ferreira VM. 2016. Effect of pozzolans with different physical and chemical characteristics on concrete properties. Mater. Construcc. 66(322):e083. https://doi.org/10.3989/mc.2016.01815

5. Bildirici ME. Ersin ÖÖ. 2024. Cement production and CO_2 emission cycles in the USA: evidence from MS-ARDL and MS-VARDL causality methods with century-long data. Environ Sci. Pollut. Res. 31:35369–35395. https://doi.org/10.1007/s11356-024-33489-2

6. López-Zaldívar O, Mayor-Lobo PL, Fernández-Martínez F, Hernández-Olivares F. 2015. Improved cement mortars by addition of carbonated fly ash from solid waste incinerators. Mater. Construcc. 65(319):e062. https://doi.org/10.3989/mc.2015.07114

7. Li J, Chen J, Bu C, Zhang M, Yu J, Yu X, Sun Y, Yu Y. 2025. Synergistic enhancement of sulfate resistance in recycled aggregate concrete through multi-pathway blocking via carbonation treatment and fly ash incorporation. Constr. Build. Mater. 491:142685. https://doi.org/10.1016/j.conbuildmat.2025.142685

8. Wang Cq, Yu L, Wang Hr, Gao Sh, Huang JS, Chen X, Shao Ms. 2025. LC50 fly ash microbead lightweight high-strength concrete: mix ratio design, stress mechanism, and life cycle assessment. Arch. Civ. Mech. Eng. 25:18. https://doi.org/10.1007/s43452-024-01066-6

9. Camargo-Pérez NR, Abellán-García J, Fuentes L. 2023. Use of rice husk ash as a supplementary cementitious material in concrete mix for road pavements. J. Mater. Res. Tech. 25:6167-6182. https://doi.org/10.1016/j.jmrt.2023.07.033

10. Kumar P, Gogineni A, Upadhyay R. 2024. Mechanical performance of fiber-reinforced concrete incorporating rice husk ash and recycled aggregates. J. Build. Rehabil. 9:144. https://doi.org/10.1007/s41024-024-00500-9

11. Suárez Silgado SS, Calderón Valdiviezo L, Betancourt Quiroga C. 2024. Life cycle analysis and economic evaluation of cement and concrete mixes with rice husk ash: application to the Colombian context. Mater. Construcc. 74(353):e335. https://doi.org/10.3989/mc.2024.350723

12. Sanit-in P, Charoensuk T, Dueramae S, Abdulmatin A, Ratanachu P, Tangchirapat W, Jaturapitakkul C. 2024. An investigation of palm oil fuel ash and limestone powder for use in sustainable high strength concrete construction. Mater. Construcc. 74(355):e351. https://doi.org/10.3989/mc.2024.372324

13. Sakri MF, Ismail R, Zakwan FAA. Hashim NH. 2025. Enhancing concrete sustainability: the role of palm oil fuel ash in improving compressive strength and reducing environmental impact. J. Build. Rehabil. 10:15. https://doi.org/10.1007/s41024-024-00524-1

14. Chalee W, Cheewaket T, Jaturapitakkul. 2021. Enhanced durability of concrete with palm oil fuel ash in a marine environment. J. Mater. Res. Tech. 13:128-137. https://doi.org/10.1016/j.jmrt.2021.04.061

15. Luna-Galiano Y, Fernández-Pereira C, Izquierdo M. 2016. Contributions to the study of porosity in fly ash-based geopolymers. Relationship between degree of reaction, porosity and compressive strength. Mater. Construcc. 66(324):e098. https://doi.org/10.3989/mc.2016.10215

16. Salaemae P, Abdulmatin A, Prachasaree W, Hawa A. 2025. Enhancing geopolymer mortars: The role of surgical face masks in modifying mechanical and thermal properties. Eng. Appl. Sci. Res. 52(1):1-16. https://doi.org/10.14456/easr.2025.1

17. Shamsah M, Kalfat R, Subramaniam KVL. 2025. Impact of low NaOH molarities on mechanical and durability properties of ambient and oven-cured fly ash geopolymer concrete. J. Build. Mater. 105:112491. https://doi.org/10.1016/j.jobe.2025.112491

18. Zhou Y, Elchalakani M, Sadakkathulla MA, Hassanli R, Guo X, Tawfik E, Youssf O. 2025. Impact of fly ash on slag-based engineered geopolymer composites: Multiple-scale investigations. Structr. 80:109751. https://doi.org/10.1016/j.istruc.2025.109751

19. Harmaji A, Jafari R, Simard G. 2025. Durable bauxite-residue geopolymers: Enhancing scaling resistance with fly ash and waste glass powder. Constr. Build. Mater. 491:142661. https://doi.org/10.1016/j.conbuildmat.2025.142661

20. Adisa MA, Odeyemi SO, Wilson UN, Subomi IS, Olarewaju AF, Adebimpe AS. 2025. Mechanical properties of geopolymer concrete with partial replacement of fly ash by agricultural waste ashes. Discov. Civ. Eng.

2:113. https://doi.org/10.1007/s44290-025-00272-2

21. Kuri JC, Nuruzzaman Md, Sarker PK. 2023. Sodium sulphate resistance of geopolymer mortar produced using ground ferronickel slag with fly ash. Cera. Int. 49(2):2765-2773. https://doi.org/10.1016/j.ceramint.2022.09.258

22. Beltrame NAM, Trisotto AV, Souto B, da Silva JCN, Pereira BCG, Medeiros-Junior RA. 2024. Effect of sulfate attack on geopolymer mortars at early ages of exposure. Mater. Struct. 57:239. https://doi.org/10.1617/s11527-024-02526-4

23. Wan-En O, Yun-Ming L, Cheng-Yong H, Abdullah MMAB, Ngee HL, Pakawanit P, Lee WH, Ken PW, Hoe-Woon T, Yu-Xin Y. 2024. Magnesium sulphate resistance of fly ash one-part geopolymers: Influence of solid alkali activators on physical, mechanical and chemical performance. Constr. Build. Mater. 446:137971. https://doi.org/10.1016/j.conbuildmat.2024.137971

24. Mehta A, Siddique R. 2017. Sulfuric acid resistance of fly ash based geopolymer concrete. Constr. Build. Mater. 146:136-143. https://doi.org/10.1016/j.conbuildmat.2017.04.077

25. Elyamany HE, Abd Elmoaty Abd M, Diab ARA. 2021. Sulphuric acid resistance of slag geopolymer concrete modified with fly ash and silica fume. Iran J. Sci. Tech. Tran. Civ. Eng. 45:2297–2315. https://doi.org/10.1007/s40996-020-00515-5

26. Ariyadasa PW, Manalo AC, Lokuge W, Aravinthan V, Gerdes A, Kaltenbach J, Galvan BA. 2024. Macro and microstructural evolution of low-calcium fly ash-based geopolymer mortar exposed to sulfuric acid corrosion. Cem. Concr. Res. 178:107436. https://doi.org/10.1016/j.cemconres.2024.107436

27. Hassan A, Arif M, Shariq M. 2019. Effect of curing condition on the mechanical properties of fly ash-based geopolymer concrete. SN Appl. Sci. 1:1694. https://doi.org/10.1007/s42452-019-1774-8

28. Zhang H, Li L, Yuan C, Wang Q, Sarker PK, Shi X. 2020. Deterioration of ambient-cured and heat-cured fly ash geopolymer concrete by high temperature exposure and prediction of its residual compressive strength. Constr. Build. Mater. 262:120924. https://doi.org/10.1016/j.conbuildmat.2020.120924

29. Hawa A, Tonnayopas D, Prachasaree W, Taneerananon P. 2013. Development and performance evaluation of very high early strength geopolymer for rapid road repair. Adv. Mater. Sci. Eng. 2013:764180. http://doi.org/10.1155/2013/764180

30. Azarsa P, Gupta R. 2020. Comparative study involving effect of curing regime on elastic modulus of geopolymer concrete. Build. 10(6):101. https://doi.org/10.3390/buildings10060101

31. Bakharev T. 2005. Resistance of geopolymer materials to acid attack. Cem. Concr. Res. 35(4):658–670. https://doi.org/10.1016/j.cemconres.2004.06.005

32. Bakharev T. 2005. Durability of geopolymer materials in sodium and magnesium sulfate solutions. Cem. Concr. Res. 35:1233–1246. https://doi.org/10.1016/j.cemconres.2004.09.002

33. Temuujin J, Minjigmaa A, Lee M, Chen-Tan N, van Riessen A 2011. Characterisation of class F fly ash geopolymer pastes immersed in acid and alkaline solutions. Cem. Concr. Com. 33(10):1086–1091. https://doi.org/10.1016/j.cemconcomp.2011.08.008

34. Ranjbar N, Mehrali M, Behnia A, Alengaram UJ, Jumaat MZ. 2014. Compressive strength and microstructural analysis of fly ash/palm oil fuel ash based geopolymer mortar. Mater. Des. 59:532-539. https://doi.org/10.1016/j.matdes.2014.03.037

35. Ahmat AM, Alengaram UJ, Shamsudin MF, Alnahhal AM, Ibrahim MSI, Ibrahim S, Rashid RSM. 2023. Assessment of sustainable eco-processed pozzolan (EPP) from palm oil industry as a fly ash replacement in geopolymer concrete. Constr. Build. Mater. 387:131424. https://doi.org/10.1016/j.conbuildmat.2023.131424

36. Nuaklong O, Sata V, Chindaprasirt P. 2018. Properties of metakaolin-high calcium fly ash geopolymer concrete containing recycled aggregate from crushed concrete specimens. Constr. Build. Mater. 161:365-373. https://doi.org/10.1016/j.conbuildmat.2017.11.152

37. Luna-Galiano Y, Cornejo A, Leiva C, Vilches LF, Fernández-Pereira C. 2015. Properties of fly ash and metakaolín based geopolymer panels under fire resistance tests. Mater. Construcc. 65(319):e059. https://doi.org/10.3989/mc.2015.06114

38. Abbass AM, Firdous R, Djobo JNY, Stephan D, Elrahman MA. 2023. The role of chemistry and fineness of metakaolin on the fresh properties and heat resistance of blended fly ash-based geopolymer. SN Appl. Sci. 5:136. https://doi.org/10.1007/s42452-023-05359-y

39. Kuri JC, Sarker PK, Shaikh FUA. 2021. Sulphuric acid resistance of ground ferronickel slag blended fly ash geopolymer mortar. Constr. Build. Mater. 313:125505. https://doi.org/10.1016/j.conbuildmat.2021.125505

40. Prasanna KM, Sharath BP, Choukade H, Shivaprasad KN, Das BB, Mahesh G. 2023. Research on setting time, compressive strength and microstructure of fly ash-based geopolymer mixture containing slag. Iran J. Sci. Tech. Tran. Civ. Eng. 47:1503–1517. https://doi.org/10.1007/s40996-022-01010-9

41. Mulapeer E, Mermerdaş K, Alzeebaree R, Sor NH. 2024. Effect of aggregate type and size on the fresh properties of self-consolidating geopolymer concrete. Int. J. Civ. Eng. 22:1753–1769. https://doi.org/10.1007/s40999-024-00972-3

42. Chindaprasirt P, Ridtirud C. 2020. High calcium fly ash geopolymer containing natural rubber latex as additive. Inter. J. GEOMATE. 18(69):124-129.

43. Hawa A, Prachasaree W. 2020. The development of compressive strength, drying shrinkage and microstructure of fly ash geopolymer with field Para rubber latex. Rom. J. Mater. 50(1):59-68.

44. Rath B, Debnath R, Paul A, Velusamy P, Balamoorthy D. 2020. Performance of natural rubber latex on calcined clay-based glass fiber-reinforced geopolymer concrete. Asian J. Civ. Eng. 21:1051–1066. https://doi.org/10.1007/s42107-020-00261-z

45. Rath B. 2022. Effect of natural rubber latex on the shrinkage behavior and porosity of geopolymer concrete. Struct. Concr. 23(4):2150-2161. https://doi.org/10.1002/suco.202000788

46. ASTM C33/C33M-16. 2016. Standard specification for concrete aggregates. ASTM International, West Conshohocken, PA, USA.

47. ASTM C109/C109M-16a. 2016. Standard test method for compressive strength of hydraulic cement mortars (using2-in. or [50-mm] cube specimens). ASTM International, West Conshohocken, PA, USA.

48. ASTM C1012/C1012M-18. 2018. Standard test method for length change of hydraulic-cement mortars exposed to a sulfate solution. ASTM International, West Conshohocken, PA, USA.

49. ASTM C490/C490M-08. 2008. Standard practice for use of apparatus for the determination of length change of hardened cement paste, mortar, and concrete. ASTM International, West Conshohocken, PA, USA.

50. Hawa A, Salaemae P, Abdulmatin A, Ongwuttiwat K, Prachasaree W. 2023. Properties of palm oil ash geopolymer containing alumina powder and field Para rubber latex. Civ. Eng. J. 9(5):1271-1288. https://doi.org/10.28991/CEJ-2023-09-05-017

51. Obeng J, Andrews A, Adom-Asamoah M, Adjei S. 2023. Effect of calcium carbide residue on the sulphate resistance of metakaolin-based geopolymer mortars. Clea. Mater. 7:100177. https://doi.org/10.1016/j.clema.2023.100177

52. Kwasny J, Aiken TA, Soutsos MN, McIntosh JA, Cleland DJ. 2018. Sulfate and acid resistance of lithomarge-based geopolymer mortars. Constr. Build. Mater. 166:537-553. https://doi.org/10.1016/j.conbuildmat.2018.01.129

53. Vafaei M, Allahverdi A, Dong P, Bassim N, Mahinroosta M. 2021. Resistance of red clay brick waste/phosphorus slag-based geopolymer mortar to acid solutions of mild concentration. J. Build. Eng. 34:102066. https://doi.org/10.1016/j.jobe.2020.102066

54. Javed U, Shaikh FUA, Sarker PK. 2024. Corrosive effect of HCl and H2SO4 exposure on the strength and microstructure of lithium slag geopolymer mortars. Constr. Build. Mater. 411:134588. https://doi.org/10.1016/j.conbuildmat.2023.134588

55. Aiken TA, Kwasny J, Sha W, Soutsos MN. 2018. Effect of slag content and activator dosage on the resistance of fly ash geopolymer binders to sulfuric acid attack. Cem. Concr. Res. 111:23-40. https://doi.org/10.1016/j.cemconres.2018.06.011

56. Hewayde E, Nehdi M, Allouche E, Nakhla G. 2006. Effect of geopolymer cement on microstructure, compressive strength and sulphuric acid resistance of concrete. Mag. Concr. Res. 58(5):321–331. https://

doi.org/10.1680/macr.2006.58.5.321

57. Osama AM. 2022. Effect of immersing geopolymer slag-fly ash mortar in sulfuric acid on strength development and stability of mass. Constr. Build. Mater. 341:127786. https://doi.org/10.1016/j.conbuildmat.2022.127786

58. Alzeebaree R, Çevik A, Nematollahi B, Sanjayan J, Mohammedameen A Gül¸san ME. 2019. Mechanical properties and durability of unconfined and confined geopolymer concrete with fiber reinforced polymers exposed to sulfuric acid. Constr. Build. Mater. 215:1015–1032. https://doi.org/10.1016/j.conbuildmat.2019.04.165

59. Nematollahi B, Qiu J, Yang EH, Sanjayan J. 2017. Microscale investigation of fiber-matrix interface properties of strain-hardening geopolymer composite. Cera. Int. 43(17):15616–15625. https://doi.org/10.1016/j.ceramint.2017.08.118

60. Sata V, Sathonsawaphak A, Chindaprasirt P. 2012. Resistance of lignite bottom ash geopolymer mortar to sulfate and sulfuric acid attack. Cem. Concr. Comp. 34(5):700-708. https://doi.org/10.1016/j.cemconcomp.2012.01.010

61. Bajpai R, Shrivastava A, Singh M. 2020. Properties of fly ash geopolymer modified with red mud and silica fume: a comparative study. SN Appl. Sci. 2:1846. https://doi.org/10.1007/s42452-020-03665-3

62. Chindaprasirt P, Rattanasak U. 2023. Calcium wastes as an additive for a low calcium fly ash geopolymer. Scientific Rep. 13:16351. https://doi.org/10.1038/s41598-023-43586-w

63. Naghizadeh A, Tchadjie LN, Ekolu SO, Welman-Purchase M. 2024. Circular production of recycled binder from fly ash-based geopolymer concrete. Constr. Build. Mater. 415:135098. https://doi.org/10.1016/j.conbuildmat.2024.135098

64. Bakharev T. 2005. Durability of geopolymer materials in sodium and magnesium sulfate solutions. Cem. Concr. Res. 35(6):1233–1246. https://doi.org/10.1016/j.cemconres.2004.09.002

65. Ye H, Chen Z, Huang L. 2019. Mechanism of sulfate attack on alkali-activated slag: The role of activator composition. Cem. Concr. Res. 125:105868. https://doi.org/10.1016/j.cemconres.2019.105868

66. Yang W, Zhu P, Liu H, Wang X, Ge X, Hua M. 2021. Resistance to sulfuric acid corrosion of geopolymer concrete based on different binding materials and alkali concentrations. Mater. 14(23):7109. https://doi.org/10.3390/ma14237109

67. Xie Y, Lin X, Ji T, Liang Y, Pan W. 2019. Comparison of corrosion resistance mechanism between ordinary Portland concrete and alkali-activated concrete subjected to biogenic sulfuric acid attack. Constr. Build. Mater. 228:117071. https://doi.org/10.1016/j.conbuildmat.2019.117071

68. Allahverdi A, Škvára F. 2005. Sulfuric acid attack on hardened paste of geopolymer cements Part 1. Mechanism of corrosion at relatively high concentrations. Ceramics – Silikaty. 49(4):225-229.

69. Sun B, Ye G, de Schutter G. 2022. A review: Reaction mechanism and strength of slag and fly ash-based alkali-activated materials. Constr. Build. Mater. 326:126843. https://doi.org/10.1016/j.conbuildmat.2022.126843

70. Yılmaz A, Degirmenci FN, Aygörmez Y. 2024. Effect of initial curing conditions on the durability performance of low-calcium fly ash-based geopolymer mortars. J. Spanish. Cer. Gla. Soc. 63(4):238-254. https://doi.org/10.1016/j.bsecv.2023.10.006

71. Ruiz-Agudo E, Putnis CV, Jiménez-López C, Rodriguez-Navarro C. 2009. An atomic force microscopy study of calcite dissolution in saline solutions: the role of magnesium ions. Geo. Cosmo. Acta 73(11):3201–3217. https://doi.org/10.1016/j.gca.2009.03.016

72. Chen K, Wu D, Xia L, Cai Q, Zhang Z. 2021. Geopolymer concrete durability subjected to aggressive environments—A review of influence factors and comparison with ordinary Portland cement. Constr. Build. Mater. 279:122496. https://doi.org/10.1016/j.conbuildmat.2021.122496

73. Shearer CR, Provis JL, Bernal SA, Kurtis KE. 2016. Alkali-activation potential of biomass-coal co-fired fly ash. Cem. Concr. Comp. 73:62-74. https://doi.org/10.1016/j.cemconcomp.2016.06.014

74. Zhang W, Yao X, Yang T, Zhang Z. 2018. The degradation mechanisms of alkali-activated fly ash/slag blend cements exposed to sulfuric acid. Constr. Build. Mater. 186:1177–1187. https://doi.org/10.1016/j.conbuildmat.2018.08.050